CHEMISTRY
A EUROPEAN JOURNAL

DOI: 10.1002/chem.200700034

Role of the Oriented Attachment Mechanism in the Phase Transformation of Oxide Nanocrystals

Caue Ribeiro,*[a] Cristiane Vila,[b] José Milton Elias de Matos,[c] Jefferson Bettini,[d] Elson Longo,[e] and Edson R. Leite[b]

Abstract: "Bottom-up" methods to obtain nanocrystals usually result in metastable phases, even in processes carried out at room temperature or under soft annealing conditions. However, stable phases, often associated with anisotropic shapes, are obtained in only a few special cases. In this paper we report on the synthesis of two well-studied oxides—titanium and zirconium oxide—in the nanometric range, by a novel route based on the decomposition of peroxide complexes of the two metals under hydrothermal soft conditions, obtaining metastable and stable phases in both cases through transformation. High-resolution transmission electron microscopy analysis reveals the existence of typical defects relating to growth by the oriented attachment mechanism in the stable crystals. The results suggest that the mechanism is associated to the phase transformation of these structures.

Keywords: crystal growth · nanostructures · oriented attachment · phase transitions

Introduction

It is generally understood that, in the synthesis of nanomaterials, many metastable structures appear to be stable in the nanometric range, without the addition of dopants or constriction by a matrix.[1] A typical case is the synthesis of TiO_2 polymorphs, anatase, brookite and rutile.[2] While several papers report on the synthesis of nanocrystalline anatase,[3–8] few report, for example, on nanocrystalline rutile.[9,10] However, several papers state that the formation of rutile passes through the three metastable phases and it has been established that rutile is the most stable TiO_2 polymorph (observations of micrometric anatase are scarce).[1,11–14]

Another case commonly reported is the synthesis of nanocrystalline zirconium oxide in the tetragonal phase. Although tetragonal zirconia appears stable only over 1175 °C, early reports confirm the stabilization of the phase below 10 nm without applied tension, and stabilization below 40 nm in a constricted matrix.[15–18] In fact, few reports exist on monoclinic zirconia in the nanometric range, except in the 15 nm-range.[19] Pitcher and co-authors discussed this transition in detail[20] based on calorimetric surface energy enthalpy measurements, showing that the average surface energy of the tetragonal phase is lower than that of the monoclinic phase. Keeping in mind that the stability of a given nucleus or small cluster is given by the balance between the free energy of formation (favorable to the nucleus formation) and the work given by the new surface (unfavorable), it is clear that lower surface energies will favor the formation of these metastable crystals in lower sizes. Garvie[15] used this argument to explain the tetragonal stabilization of nanocrystals at room temperature, developing a

[a] Dr. C. Ribeiro
EMBRAPA Instrumentação Agropecuária
Rua XV de Novembro, 1452-3560-970, CP 741
São Carlos, SP (Brazil)
Fax: (+55) 16-3372-5958
E-mail: caue@cnpdia.embrapa.br

[b] Dr. C. Vila, Prof. Dr. E. R. Leite
LIEC/Universidade Federal de São Carlos
Departamento de Química
Rod. Washington Luiz, km 235-13565-905
São Carlos, SP (Brazil)

[c] Dr. J. Milton Elias de Matos
Universidade Federal do Piauí
Departamento de Química
Campus Min. Petrônio Portela, 64049-550
Teresina, PI (Brazil)

[d] Dr. J. Bettini
Laboratório Nacional de Luz Sincroton (LNLS)
CP 6192-13084-971, Campinas, SP (Brazil)

[e] Prof. Dr. E. Longo
LIEC/Universidade Estadual Paulista
Instituto de Química
Rua Francisco Degni, s/n, 14800-900
Araraquara, SP (Brazil)

thermodynamic approach to determine a critical size for the phase stabilization.

However, the application of thermodynamic approach to titania crystals is problematic. In principle, anatase is metastable in relation to rutile at any temperature,[2,21] although the energetics of anatase to rutile transformation can be estimated for a given temperature.[2,12] However, to the best of our knowledge, no one has managed to apply Garvie's approach[15] successfully to determine a critical size of this transformation. Gribb and Banfield[22] experimentally observed a critical size of 14 nm for the stability of anatase crystals, but phase transformation occurred at larger sizes and the resulting rutile nanocrystals grew relatively faster. In fact, anatase nanocrystals are commonly observed in sizes below 15 nm,[23–26] although several sizes, from 15 to 50 nm,[13,24] have also been reported in the literature, a fact that is explained by the dependence of anatase stabilization of several parameters, such as starting material, synthesis environment and temperature.

An interesting generalization of the discussion is to assume that phase stability depends on global thermodynamic parameters, that is, the total surface energy of the particle as a function of the volume. Barnard and Zapol[13,14,27,28] and Barnard et al.[29,30] engaged in similar discussions, obtaining a general expression for the free energy G_x^0 of an arbitrary nanoparticles, taking in account the balance of surface energy as a function of the exposed crystallographic planes, as follows:

$$G_x^0 = G_x^{\text{bulk}} + \frac{M}{\rho_x}(1-e)q\sum f_i\gamma_i(T) \quad (1)$$

where the first term is defined as the standard free energy of formation, $G_x^{\text{bulk}} = \Delta G_x^0(T)$, and the second term is expressed in terms of surface energy γ_i for each i plane on the surface and molar surface area A—which can be described using the relations of density of the phase $x(\rho_x)$, molar mass M, the volume dilation of the nanoparticle e (negligible in several cases), the surface to volume ratio q and f_i, a weight factor of the facets i in the crystal ($\Sigma f_i = 1$). In the above formulation, the expression takes into account the crystallographic alignment of the properties and, indirectly, the shape. We can sum, in this formulation, the contributions of factors as the interaction with ions in surface (counterions, surfactants, etc.) as a way to minimize energy in specific crystallographic planes.

Thus, the growth mechanisms of nanocrystals can play an important role in phase transformation. Many works associate the growth of nanocrystals to the Ostwald ripening mechanism,[25,31,32] which is a dissolution–reprecipitation growth mechanism.[33] In this mechanism the particles tend toward an isotropic growth, generating particles with regular, almost spherical shapes. Hence, variations in the weight factor f_i of the facets are not expected. However, recent investigations into oriented attachment crystal growth[26,34,35] have demonstrated that this mechanism favors the formation of anisotropic nanocrystals by the coalescence of two or more nanocrystals.[36,37] Previous theoretical works[38–40] emphasized that the mechanism is faster than the diffusional mechanism, particularly in the early stages of growth. Thus, one can assume that the fast growth and the anisotropic shapes obtained can give rise to other phenomena relating to shape and size, such as spontaneous phase transformation. In this work, we show that the phase transformation of two well-known oxide systems—titania and zirconia—is followed by crystal growth by the oriented attachment mechanism. To this end, we used a hydrothermal route under soft conditions, which enabled us to correlate the growth mechanism and the phase transformation. These results can shed further light on the discussion about phase transformation and stability in nanocrystals, highlighting the importance of growth mechanisms and underpinning synthetic strategies and technological applications.

Results and Discussion

The characterization of TiO_2 nanocrystals morphology is shown in Figure 1a. The rod-like rutile crystals are largely identified, in contrast with a few bipyramidal particles characteristic of anatase phase, dispersed in small crystals. In general, the rutile crystals (shown in details in Figure 1b and c) have no determined diameter or length, as can be seen in distribution presented on Figure 2 (taking in account only the rod fraction, that is, rutile nanoparticles). Notably the average diameter of these rods is around 10 nm, which is below the stability size for the anatase phase reported in the literature[22,25] of 14 nm—even for a colloid treated for longer than 48 h. A substantial fraction of the overall distribution ($\approx$10%) presented a particle size of less than 10 nm, maintaining the rod-shape. In fact, the shape factor of the particles is almost constant, $l/\varnothing \approx 5$, showing that the growth mechanism governing the larger particles was probably the same as that in the smaller ones. From Figure 2 it is also evident that the evolution of the crystal size was preferentially longitudinal.

An analysis of Figure 1b and c reveals several line defects along the length of the particle, which are characteristic of the oriented attachment mechanism and evidence of growth by this mechanism (see white dotted arrows). The twin boundaries visible in Figure 1c illustrate the growth mechanism oriented longitudinally. Apparently, the mechanism acts preferentially on longitudinal growth, causing the nanorod to grow to [110], although lateral growth is not unusual, as indicated in Figure 1c, which illustrates the statistical nature of the oriented attachment. In Figure 1d a detailed view of the nanorod reveals the side attachment of a 6 nm nanorod, which gives evidence for the role of the growth mechanism in the formation of large nanorods. This result is consistent with the apparent constant shape factor of the particles as discussed earlier.

Following the calculations of Barnard and Zapol,[13] the (110) are the lower energy planes in rutile, which is consistent with their suggested predominance, minimizing the

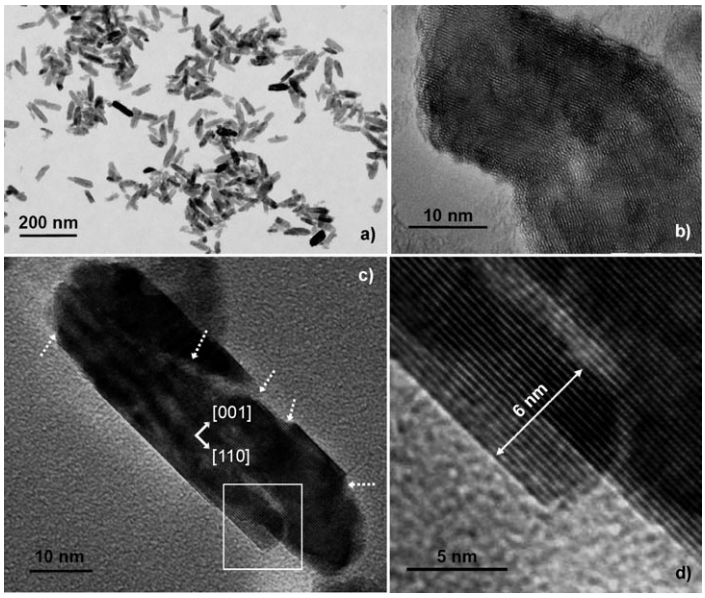

Figure 1. TEM and HRTEM images of TiO_2 nanoparticles obtained by PCT gel decomposition: a) BF image of the particles; b) rutile nanorod showing twin boundary in the length; c) rutile nanorod showing several characteristic defects of oriented attachment growth mechanism; d) inset of c) showing a side-coalesced nanorod.

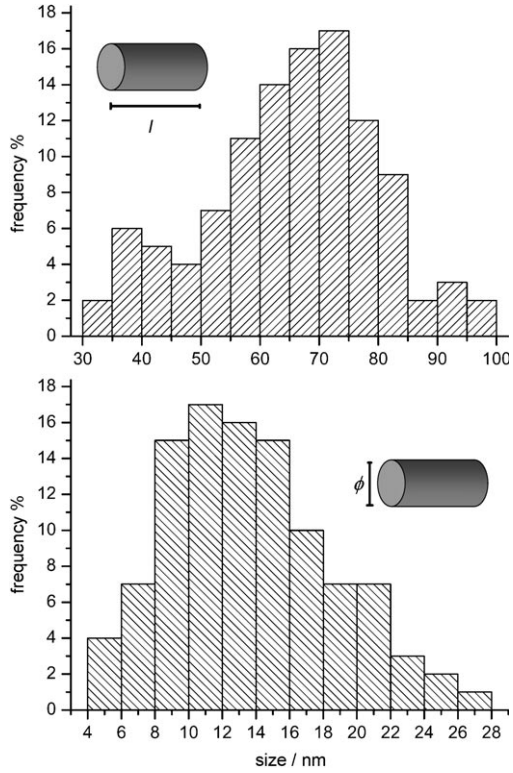

Figure 2. Length and diameter ($\varnothing$) distribution of rutile nanorods. Only the nanorod fraction was estimated.

total surface energy of the rod (the nanorods sides are (110), as seen in Figure 1). Importantly the weight factor [as defined in Eq. (1)] of (110) planes is approximately the same for any nanorod, since the shape factor is assumed to be constant.

Figure 3 shows TEM and HRTEM images of ZrO_2 nanocrystals obtained here. Acicular nanoparticles (needle-shaped) were generally observed (white dotted arrows), with a lateral size $\approx$5 nm and variable length, and some randomly dispersed near-spherical particles (white arrows). The acicular morphology is similar to that found in rutile nanocrystals, but the particles appear as coalesced in one terminal, unlike what is observed in TiO_2 nanoparticles. The distance upon planes (3.2 Å) in the length is consistent with ($\bar{1}11$) of baddeleyte phase (monoclinic), and in the diameter (5.1 Å), with (100), identifying the growth direction of the particle as [100] in length and [$\bar{1}11$] in diameter. Since the surface is not orthogonal to the growth direction, the majority surface plane is not necessary ($\bar{1}11$); in fact, the majority plane is (111) (2.85 Å), as indicated in Figure 3d.

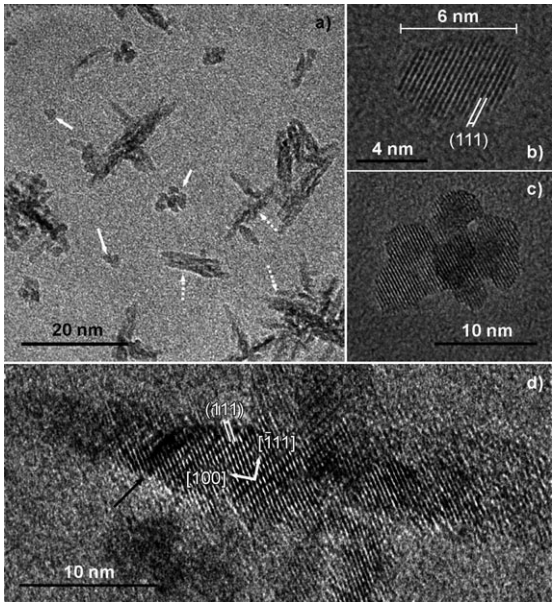

Figure 3. TEM and HRTEM images of ZrO_2 nanoparticles obtained by degradation of PCZ gel: a) BF image of the particles, showing several tetragonal (white arrows) and monoclinic (white dotted arrows) particles; b) an isolated tetragonal nanoparticle; c) a coalesced tetragonal nanoparticle, with eight pristine nanoparticles; d) an isolated monoclinic nanoparticle. The black arrow shows a stress line.

In near-spherical particles, as depicted in Figure 3b, the surface planes are identified as (111) tetragonal phase (2.9 Å). Despite the congruence, these data are not conclusive, since it can be identified with (111) badelleyte phase. However, according to Garvie,[15] the average size of these particles ($\approx$6 nm) is below the critical size expected to tetragonal phase (10 nm), and we can assume these particles to be tetragonal ZrO_2 phase. Notably this phase is minor as indicated in Figure 3a.

These particles clear undergo coalescence to form larger particles, as indicated in Figure 3c. In principle, the growth itself may be solely responsible for the phase transformation

(tetragonal to monoclinic); however, the agglomerate in Figure 3c remained in the tetragonal phase, indicating possible constraining effects (interfacial discordances) due to defects associated to oriented attachment mechanism. Similarly, other coalesced particles are visible in Figure 3a (white arrows). However, a closer examination of Figure 3d reveals the same characteristic defects that are visible in monoclinic nanoparticle. The size distribution (length and diameter, Figure 4) is uniform, like that observed in rutile nanoparticles, with an average diameter size ranging from 4 to 5 nm, that is, smaller than the reported critical size.

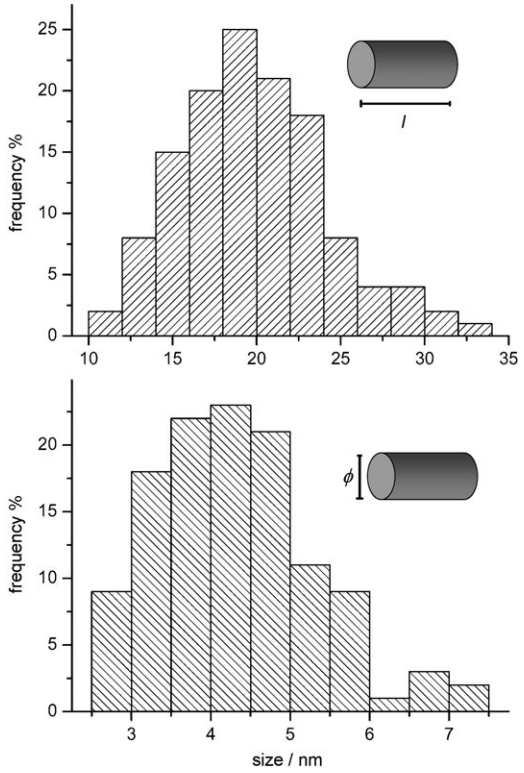

Figure 4. Length and diameter ($\varnothing$) distribution of monoclinic neddle-like nanoparticles.

These results are very consistent with the calculations of Barnard et al.[30] for several ZrO_2 nanocrystal shapes. The authors identified an "optimized" nanomorphology for the tetragonal phase that can be identified with the near-spherical tetragonal nanoparticles. The results revealed the highest transition sizes (12.7 nm) for this structure, compared with the anisotropic shapes. In fact, the calculations also show that a "optimized" monoclinic nanocrystal—close to a bipyramid shape, a anisotropic shape—can be stable with size $\approx$4 nm, as observed in Figures 3 and 4.

Our X-ray diffraction data merit a general discussion, since the values obtained can be considered the average value of the entire sample. Figure 5 shows the XRD patterns for phase formation in titania and zirconia synthesis. Anatase nanocrystals appears as preferential only in shorter treatment times, and the rutile formation is predominant in the sample treated over 24 h, as seen in Figure 5. The synthesized zirconia nanocrystals showed a well-formed baddeleyte phase (monoclinic), while the tetragonal phase was not detect even after short thermal treatment times. This is consistent with Figure 3 and is in accordance with the Ostwald step rule.[1]

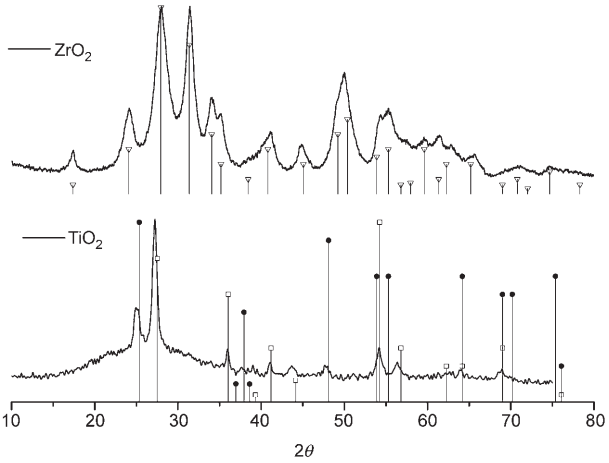

Figure 5. X-ray diffraction of as-synthesized nanocrystals (TiO_2 and ZrO_2), treated over 24 h. ▽: baddeleyite, □: rutile, ●: anatase.

The particles sizes were estimated using Scherrer's formula[41] for each identified crystallographic plane in the diffraction patterns, as indicated in Table 1. Note the congruence of the calculated data and the TEM images in Figures 1 and 3: the rutile nanoparticles were estimated in 14.5 nm in [110]; this value is lower than that estimated as the average length, but is a good indication of the size of primary rutile nanocrystals. The difference between the calculated values (from 9.8 to 29.1 nm) shows the system's anisotropy. The values calculated for the remnant anatase nanocrystals are consistent with those reported in the literature. For zirconia nanocrystals, the data are in surprisingly good agreement with the statistical size (Figure 4), $l = 15$ nm (corresponding to [100] and $\varnothing = 5.2$ nm (corresponding to $[\bar{1}11]$).

As determined by Christensen and Carter,[42] the lower energy planes in monoclinic zirconia are $(\bar{1}11)$, which are predominant. Following the authors, the Wulff construction of the tetragonal crystal predicts the predominance of {111}

Table 1. Particle size in function of crystallographic coherence according Scherrer's formula.

Anatase			Rutile			Monoclinic		
	2θ	Size [nm]		2θ	Size [nm]		2θ	Size [nm]
[101]	25	8.2	[110]	28	14.5	[100]	17	15.0
[200]	48	12.2	[101]	36	29.1	[110]	24	7.1
			[111]	41	22.3	$[\bar{1}11]$	28	5.2
			[210]	44	9.8	[111]	31	8.6
			[220]	57	12.1	[020]	34	8.87

facets, which is actually visible in Figure 3. Since the martensitic tetragonal → monoclinic transformation is a dislocation event,[15–17] it is expected that $t\{111\}$ facets are converted into $m\{111\}$ and $m\{\bar{1}11\}$, because these are parallel planes. However, $m\{\bar{1}11\}$ is the most stable plane, and not $m\{111\}$. Therefore, their predominance in facets may be the main reason for the needle-like shape, since the growth mechanism would not favor sideway growth.

Based on this argument, it is clear that the phase transformation in zirconia occurred after successive coalescence events of tetragonal nanoparticles in [100], although coalescence in other directions is not impossible, as indicated in Figure 3c. However, the phase change only occurs if the total surface energy of the coalesced nanocrystal is favorable for the transformation, which is more probable in anisotropic nanocrystals, as predicted by Equation (1). This is consistent with the preferential coalescence of the monoclinic nanocrystals observed in the terminals, with few lateral coalescence events. Finally, Figure 3d shows a stress line (black arrow) near the defects associated with oriented attachment, which may have resulted from the transformation in the crystals formed here.

In the case of rutile nanocrystals, this discussion is more complex since the anatase to rutile transition is known as a nucleation–growth process.[21] In this case, it is difficult to state that the phase transformation occurs after the coalescence event, or that the attachment acts by stabilizing some randomly formed "unstable" rutile nanocrystals. Zhang and Banfield[43,44] suggested that the mechanism of the anatase to rutile phase transformation is dominated by interface nucleation in temperatures below 873 K. This suggestion is consistent with the kinetic study of Shannon and Pask,[21] who reported on the surface nucleation of rutile in coarsely crystalline anatase. It is therefore logical to assume that rutile phase nucleation begins during coalescence events, by interfacial nucleation at the common boundary of the coalesced particles, in which case the growth process should play a decisive role in stabilizing the desired phase. This proposition still requires an in-depth investigation to validate it.

Finally, it is obvious that phase stabilization via surface energy is highly dependent on the particles morphology and plane surface distribution. It is common to describe phase transformation as a crossover in free energy–diameter size of the particles of the two phases, defining a critical size.[1] These results demonstrate the importance of the crossover in total surface energy per volume, which is the characteristic size of the phases. It should be noted that the role of oriented attachment is to modify the area/volume relation in the formed particles, favoring or not the phase transformation according the exposed crystallographic planes after the event. In fact, previous works have demonstrated highly anisotropic metastable phases, demonstrating this possibility.[34] Thus, in the case of nanorods/needle-like particles, the characteristic size can be assumed to be the length. Keeping in mind that the contribution of the side planes will increase with the length, and assuming these planes are less energetic, the surface energy to volume ratio will decline continuously with the length, stabilizing the phase even in thin diameters (below the reported critical size) as observed in this study.

Summary

The two cases of phase stability in nanometric range observed in this work show that phase stability is strongly dependent on the minimization of the total surface energy. This minimization can be attained by tailoring highly anisotropic crystals, favoring planes with low energy. This goal is also achieved in systems in which counterions or surfactants can stabilize some surfaces, reducing the effective surface energy. The oriented attachment mechanism can interfere by forming anisotropic particles, particularly in cases where growth occurs preferentially in the high energy planes. The phase transformation will then occur by a lattice distortion process: the case of tetragonal → monoclinic transformation in zirconia, or by a nucleation-growth process. In cases where interfacial nucleation is preferable, as in anatase → rutile transition, the common boundary between the two attached particles can be a nucleation site. This information is important to establish the role of oriented attachment in phase stability: stabilization of metastable phases probably relies on methods to prevent growth by oriented attachment, whereby the stabilization of stable phases in nanometric range can be accelerated by inducing oriented attachment on the particles' high energy planes.

Experimental Section

Titanium and zirconium oxides were synthesized by the hydrothermal treatment of the peroxo complexes of titanium (PCT) and zirconium (PCZ) gel solution. The PCT gel was prepared from a titanium(IV) isopropoxide ($Ti(OCH(CH_3)_2)_4$, Aldrich, USA) and H_2O_2 (Mallinckrodt Baker, USA, 30 % in volume). In a typical synthetic process, titanium isopropoxide (2.84 g) was added slowly to a H_2O_2 solution (11.3 g of a solution 30 wt % H_2O_2) (10:1 % mol H_2O_2/Ti) under vigorous stirring in an ice bath. The final volume of the solution was then adjusted using distilled water (100 mL), and poured into a round-bottomed flask. The flask was connected to a reflux apparatus to prevent water evaporation and allowed to release O_2 produced by the decomposition of excess H_2O_2. The solution was kept under reflux at 80 °C for 15 min, resulting in a transparent yellow gel. The PCZ gel was obtained following a similar procedure: zirconyl(IV) nitrate (1.16 g $ZrO(NO_3)_2{\cdot}xH_2O$, Acros) was added to a H_2O_2 solution (2.55 g of a 30 wt % solution) (15:1 % mol H_2O_2/Zr), resulting in a colorless, slightly viscous solution without any refluxing process. The solution was kept under vigorous stirring for 15 min to allow for the release of O_2.

Both the gels (10 g) were dissolved in water (90 g) and the resulting solution (with pH 3) was poured into a bottle with an autoclavable screw cap. The bottle was then placed in a regular laboratory oven and subjected to a constant temperature (95 °C for PCT gel and 130 °C for PCZ gel) for 48 h.

The morphology and particle size distribution of both systems were characterized using a 300 kV transmission electron microscope (JEOL 3010, LNLS facility). The particle size distribution was estimated based on the measurements of TEM images of at least 200 particles. The TEM samples

were prepared by wetting carbon-coated copper grids with a drop of the colloidal suspensions for 20 s, followed by drying in air. The X-ray diffraction patterns were carried out in a Rigaku D-Max 2500 diffractometer with CuKα radiation, in a scanning routine of $1°\,min^{-1}$, to define the peak position and width.

Acknowledgement

The authors gratefully acknowledge the financial support of the Brazilian research funding agencies FAPESP and CNPq. HRTEM microscopy facilities were provide by LNLS-Campinas,SP, Brazil.

[1] A. Navrotsky, *Proc. Natl. Acad. Sci. USA* **2004**, *101*, 12096–12101.
[2] A. Navrotsky, O. J. Kleppa, *J. Am. Ceram. Soc.* **1967**, *50*, 626–630.
[3] E. A. Barringer, H. K. Bowen, *Langmuir* **1985**, *1*, 414–420.
[4] J. H. Jean, T. A. Ring, *Langmuir* **1986**, *2*, 251–255.
[5] T. E. Mates, T. A. Ring, *Colloids Surf.* **1987**, *24*, 299–313.
[6] L. Kavan, K. Kratochvilova, M. Grätzel, *J. Electroanal. Chem.* **1995**, *394*, 93–102.
[7] T. J. Trentler, T. E. Denler, J. F. Bertone, A. Agrawal, V. L. Colvin, *J. Am. Chem. Soc.* **1999**, *121*, 1613–1614.
[8] G. Garnweitner, M. Antonietti, M. Niederberger, *Chem. Commun.* **2005**, *3*, 397–399.
[9] J. Ragai, W. Lotfi, *Colloids Surf.* **1991**, *61*, 97–109.
[10] S. Han, S. H. Choi, S. S. Kim, M. Cho, B. Jang, D. Y. Kim, J. Yoon, T. Hyeon, *Small* **2005**, *1*, 812–816.
[11] H. Z. Zhang, J. F. Banfield, *Chem. Mater.* **2002**, *14*, 4145–4154.
[12] M. R. Ranade, A. Navrotsky, H. Z. Zhang, J. F. Banfield, S. H. Elder, A. Zaban, P. H. Borse, S. K. Kulkarni, G. S. Doran, H. J. Whitfield, *Proc. Natl. Acad. Sci. USA* **2002**, *99*, 6476–6481.
[13] A. S. Barnard, P. Zapol, *J. Phys. Chem. B* **2004**, *108*, 18435–18440.
[14] A. S. Barnard, P. Zapol, *Phys. Rev. B* **2004**, *70*, 235403.
[15] R. C. Garvie, *J. Phys. Chem.* **1965**, *69*, 1238–1243.
[16] R. C. Garvie, *J. Am. Ceram. Soc.* **1972**, *55*, 303–305.
[17] R. C. Garvie, *J. Phys. Chem.* **1978**, *82*, 218–224.
[18] S. Shukla, S. Seal, *J. Phys. Chem. B* **2004**, *108*, 395–3399.
[19] G. Y. Guo, Y. L. Chen, *J. Solid State Chem.* **2005**, *178*, 1675–1682.
[20] M. W. Pitcher, S. V. Ushakov, A. Navrotsky, B. F. Woodfield, G. Li, J. Boerio-Goates, B. M. Tissue, *J. Am. Ceram. Soc.* **2005**, *88*, 160–167.
[21] R. D. Shannon, J. A. Pask, *J. Am. Ceram. Soc.* **1965**, *48*, 391–398.
[22] A. A. Gribb, J. F. Banfield, *Am. Mineral.* **1997**, *82*, 717–728.
[23] C. Kormann, D. W. Bahnemann, M. R. Hoffmann, *J. Phys. Chem.* **1988**, *92*, 5196–5201.
[24] K. Yanagisawa, J. Ovenstone, *J. Phys. Chem. B* **1999**, *103*, 7781–7787.
[25] G. Oskam, A. Nellore, R. L. Penn, P. C. Searson, *J. Phys. Chem. B* **2003**, *107*, 1734–1738.
[26] R. L. Penn, G. Oskam, T. J. Strathmann, P. C. Searson, A. T. Stone, D. R. Veblen, *J. Phys. Chem. B* **2001**, *105*, 2177–2182.
[27] A. S. Barnard, P. Zapol, *J. Chem. Phys.* **2004**, *121*, 4276–4283.
[28] A. S. Barnard, P. Zapol, L. A. Curtiss, *J. Chem. Theory Comput.* **2005**, *1*, 107–116.
[29] A. Barnard, Z. Saponjic, D. Tiede, T. Rajh, L. Curtiss, *Rev. Adv. Mater. Sci.* **2005**, *10*, 21–27.
[30] A. S Barnard, R. R Yeredla, H. Xu, *Nanotechnology* **2006**, *17*, 3039–3047.
[31] G. Oskam, Z. S. Hu, R. L. Penn, N. Pesika, P. C. Searson, *Phys. Rev. E* **2002**, *66*, 011403.
[32] F. Huang, H. Z. Zhang, J. F. Banfield, *Nano Lett.* **2003**, *3*, 373–378.
[33] I. M. Lifshitz, V. V. Slyozov, *Phys. Chem. Solids* **1961**, *19*, 35–50.
[34] R. L. Penn, J. F. Banfield, *Geochim. Cosmochim. Acta* **1999**, *63*, 1549–1557.
[35] C. Ribeiro, E. J. H. Lee, T. R. Giraldi, R. Aguiar, E. Longo, E. R. Leite, *J. Appl. Phys.* **2005**, *97*, 024313.
[36] J. Polleux, N. Pinna, M. Antonietti, M. Niederberger, *Adv. Mater.* **2004**, *16*, 436–439.
[37] E. J. H. Lee, C. Ribeiro, E. Longo, E. R. Leite, *J. Phys. Chem. B* **2005**, *109*, 20842–20846.
[38] C. Ribeiro, E. J. H. Lee, E. Longo, E. R. Leite, *ChemPhysChem* **2005**, *6*, 690–696.
[39] T. O. Drews, M. A. Katsoulakis, M. Tsapatsis, *J. Phys. Chem. B* **2005**, *109*, 23879–23887.
[40] C. Ribeiro, E. J. H. Lee, E. Longo, E. R. Leite, *ChemPhysChem* **2006**, *7*, 664–670.
[41] B. D. Cullity, *Elements of X-Ray diffraction*, Addison-Wesley, New York, **1978**.
[42] A. Christensen, E. A. Carter, *Phys. Rev. B* **1998**, *58*, 8050–8064.
[43] H. Z. Zhang, J. F. Banfield, *J. Phys. Chem. B* **2000**, *104*, 3481–3487.
[44] H. Z. Zhang, J. F. Banfield, *J. Mater. Res.* **2000**, *15*, 437–448.

Received: January 9, 2007
Published online: April 19, 2007

